Vertical β-Ga_2O_3 Schottky Rectifiers with 750 V Reverse Breakdown Voltage at 600K

Xinyi Xia[1], Minghan Xian[1], Patrick Carey[1], Chaker Fares[1], Fan Ren[1], Marko Tadjer[2], S. J. Pearton [3], Thieu Quang Tu[4], Ken Goto[5] and Akito Kuramata[4]

[1]Department of Chemical Engineering, University of Florida, Gainesville, FL 32611, USA

[2]Naval Research Laboratory, Washington DC 20375, USA

[3]Department of Materials Science and Engineering, University of Florida, Gainesville FL 32611, USA

[4]Novel Crystal Technology, Inc., Saitama, Sayama-Shi, Japan

[5]Department of Applied Chemistry, Tokyo University of Agriculture and Technology, Koganei, Tokyo 184-8588, Japan

Abstract

Field-plated vertical Ga_2O_3 rectifiers were operated up to 600K with reverse breakdown voltage (V_B) of 750 V, 950 V at 500K and 1460 V at 400K. The barrier height was 1.3 eV at 300K and reduced to 0.7 eV at 600K, with ideality factors of 1.05±0.05 and 2±0.1, respectively at these temperatures. On-state resistance, R_{ON}, was 13 mΩ.cm^2 at 300K and 41 mΩ.cm^2 at 600K, leading to respective Baliga figures of merit of 151 MW.cm^{-2} (300K) and 13.9 MW.cm^{-2} (600K). The on-off ratio was >10^4 for all temperatures measured. The leakage current showed a good fit to the thermionic field emission model when the reverse voltage was less than 80 V, and it was dominated by the tunneling effect at higher voltage. The transition voltage from thermionic emission to tunneling effect decreased as the temperature increased. At high reverse voltage, a large number of electrons are injected into the drift region, and the current shows an $I \propto V^n$ relationship with voltage, indicating a trap-assisted space-charge-limited conduction (SCLC) mechanism. We observed this SCLC relation when the reverse voltage was larger than

400 V for 500 K and 600 K. The associated trap energies for these two regions were extracted as 0.2 and 0.4 eV, consistent with levels in the gap.

Introduction

The development of power electronics technology based on wide bandgap semiconductors is attracting much interest because of the potential for significantly higher switching efficiency and ability to operate at higher powers and temperatures. Within the next decade, about 80% of all US electricity is expected to flow through power electronics. These include power distribution systems, electric vehicle fast chargers, data center power supplies, ship power systems, and renewable wind/solar energy integration. Both SiC and GaN power electronics are now commercialized and provide more efficient performance than conventional Si-based devices [1-3]. The combination of high breakdown voltage, low on-state resistance and lower switching losses is improved in the ultra-wide bandgap semiconductors [4-10] [such as Ga_2O_3, diamond, and AlN). This leads to their high Baliga's figure of merit (BFOM), defined as $\varepsilon.\mu.E_c^3$, where ε, μ, and E_c are the dielectric constant, carrier mobility, and critical breakdown field strength, respectively.

Among these ultra-wide bandgap semiconductors, monoclinic gallium oxide (β-Ga_2O_3) has recently attracted increasing attention due to the availability of high quality, large diameter single crystals from mature melt growth methods and its attractive material properties of wide E_G of 4.6–4.9 eV, good electron mobility (>200 cm^2/Vs) and estimated critical breakdown field, E_c , of~ 8 MV/cm, yielding a relatively high BFOM (>3000) with respect to silicon [11-23]. Compared to other ultra-wide bandgap materials, the inexpensive substrates lower the manufacturing cost for β-Ga_2O_3 power devices for applications requiring high operation voltage and high energy conversion efficiency.

A large literature on demonstration of power devices in this materials system now exists, including vertical and lateral MOSFETs and rectifiers [6-43]. The absence of practical p-type doping may be alleviated by use of other p-type oxide semiconductors to form a pn heterojunction with Ga_2O_3, such as NiO, Cu_2O, CuI and Ir_2O_3[27-34]. Some notable recent advancements in device performance for Ga_2O_3 diodes includes a 5A/700V junction Schottky barrier diode implemented with p-type NiO layer [35], 1.86kV p-n junction diode with NiO heterojunction [36], as well as demonstrations of >100A of absolute forward current using conventional field-plated Schottky diodes [37].

Wide energy bandgap materials are suitable for high temperature as well as high breakdown voltage applications. The ability to operate at high temperature enables wide bandgap devices to be attractive in terms of reduced package size and minimal requirement for cooling. Hindered by its low thermal conductivity, demonstrations of operation at high temperature for β-Ga_2O_3 are fairly limited. Wang et al.[38] reported operation up to 600K of rectifiers with beveled edge termination and spin-on glass passivation, achieving breakdown voltage of ~500V at this temperature. One way to increase the breakdown voltage is to grow thicker layers, but to date, the maximum drift layer thickness has been 30 µm, thinned to 20µm after the chemical mechanical planarization (CMP) step needed to achieve a flat surface morphology [15].

In this work, we report operation of field plated Schottky barrier diodes up to 750 V at 600K, with reasonable leakage current density. This was achieved by growing a 40 µm thick drift layer, thinned to 30 µm after CMP, as well as lower carrier concentration. The devices exhibit a negative temperature coefficient of breakdown and reverse leakage dominated by thermionic field emission when the reverse voltage was less than 80 V, and by tunneling conduction at higher voltage.

Experimental

The drift region of the material consisted of a 30 μm thick, lightly Si doped epitaxial layer grown by halide vapor phase epitaxy (HVPE) with minimum carrier concentration of 1.6×10^{16} cm^{-3} (the maximum was ~$3x10^{16}$ cm^{-3}), and this epitaxial layer was grown on a (001) surface orientation Sn-doped β-Ga_2O_3 single crystal (Novel Crystal Technology, Japan). The HVPE layer is actually grown initially to a thickness of ~ 40 μm, but then chemically mechanically polished to planarize the surface by removing ~10 μm of material. As seen in the Nomarski images of Figure 1, this produces a much smoother surface relative to the as-grown morphology, but there is still some surface roughness after the CMP step. It is important to note that this is a unique growth, the thickest ever attempted at NCT and the process is not optimized.

A full area Ti/Au backside Ohmic contact was formed by e-beam evaporation and was annealed at 550°C for 30s under N_2 ambient. 40 nm of Al_2O_3 and 400 nm of SiN_x were deposited as field plate dielectric using Cambridge-Nano-Fiji ALD and PlasmaTherm PECVD tools. Dielectric windows of 40 μm ×40 μm was opened using dilute buffered oxide etchant (BOE), and a 200nm Ni/Au Schottky contact was deposited with E-beam after lithography pattern followed by standard acetone lift-off. Figure 2 shows a photograph and device geometry of fabricated diodes, respectively. Of the 121 devices on this chip, approximately 46 have very smooth morphology, but this was not the only parameter that correlated with achieving high breakdown voltage. We had a yield of ~15% (~20 devices out of 121) with breakdown in the range 745-754V. The carrier concentration of these highest breakdown voltages was typically < $2x10^{16}$ cm^{-3} with no visible surface defects within the active area of the device. The remaining surface defects are due to the incomplete smoothing of the surface of the HVPE-grown layer.

The current-voltage (I-V) characteristics were recorded at 1MHz with a Tektronix 370-A curve tracer was used for forward and reverse current measurements over the temperature range 300-600K on a temperature-controlled stage. No hysteresis was observed in any of the rectifier characteristics. The forward direction was dominated by the thermionic emission (TE) current, while in the reverse direction, the thermionic field emission (TFE) and tunneling currents played an important role at high reverse bias. To extract the barrier height (Φ_b) and ideality factor (n), we used the relationship for current density in TE theory, given by [1,3,38]

$$J = J_0 \exp (eV_A/nkT) [1-\exp (-eV_A/ kT)$$

where $J_0 = A^* m_{eff}/m_0 T^2 \exp(\Phi_B /kT)$, e is electronic charge and A^* is the Richardson constant and V_A is the bias voltage applied. The magnitude of the series resistance can also be obtained from plots of $d(V_A)/d(\ln J)$ versus J, while the barrier height is obtained from $(kT/e) \ln(A^*T^2/J_0)$ [44,45]. The built-in voltage can be obtained from the C-V characteristics [45]. The fact that thermionic field emission was the dominant current transport mechanism over most of the conditions investigated can be established by the fact that the tunneling parameter E_{00}/kT was ~1 [42], where E_{00} is given by $(eh/4\pi)[N_D/m^* \varepsilon_r]^{0.5}$ and h is Planck's constant and ε_r is the relative dielectric constant. If this parameter is much less than unity, then thermionic emission is significant and field emission is dominant if this parameter is >> 1.

Capacitance-Voltage (C-V) characteristics were recorded with an Agilent 4284A Precision LCR Meter. The diode on/off ratio is another figure-of-merit was measured when switching from 2V forward to reverse biases up to 100V. The reverse breakdown voltage was defined as the bias for a reverse current of 1mA.

Results and Discussion

The barrier height was 1.23 eV at 300K and reduced to 0.7 eV at 600K, with ideality factors of 1.05±0.5 and 2±0.1, respectively at these temperatures, extracted from the I-V-T characteristics in Figure 3 and those parameters plotted in Figure 4. It is commonly observed that the barrier height decreases with increasing temperature, as it is easier for electrons to pass over the barrier since with pure thermionic emission there would be a reduced barrier at elevated temperatures. This will lead to contributions from other transport mechanisms and the commonly observed higher ideality factors at elevated temperatures. [42]. There may also be contributions from spatial inhomogeneity of the Schottky barrier [42].

The temperature coefficient was $-(2.1 \pm 0.6) \times 10^{-3}$ eV/K, which is the same order of magnitude as the temperature dependence of the band gap, namely ($-$ $4.5\text{x}10^{-3}$) eV/K [40]. In Si, the temperature coefficient of the barrier height also depends on the chemical nature of the metal, in contradiction with models suggesting Fermi-level pinning at the center of the semiconductor's band gap [41]. In Ga_2O_3, the situation is more complex, with the dependence of barrier height om metal work function being a function of the orientation of the Ga_2O_3 surface. It is generally the case that a number of factors also have an influence on barrier height and its temperature dependence. For Ga_2O_3, these factors include the interface crystallography, contact inhomogeneities, the recombination velocities on different surface planes of Ga_2O_3 or for different polytypes. For example, Lyle et al [42] found a strong positive correlation between the calculated Schottky barrier heights and the work function of metal contacts on (100) β-Ga_2O_3, in contrast to (201) β-Ga_2O_3 . Similarly, there were mixed results for (010) β-Ga_2O_3 [42]. The temperature dependence of barrier height and ideality factor in our devices is consistent with previous reports [38, 43]. We did not observe any significant change in carrier concentration as a result of the temperature cycling, as judged from the C-V measurements.

The on-state resistance of the rectifiers, R_{ON}, was 13 mΩ.cm^2 at 300K and 41 mΩ.cm^2 at 600K, leading to respective Baliga figures of merit of 150 MW.cm^{-2} (300K) and 14 MW.cm^{-2} (600K). The highest previous result was 4 MW. cm^{-2} at 600K [38]. The series resistance of the highest breakdown voltage rectifiers was typically between 200-300 Ω. The on-off ratio is another figure of merit in that having high on-current and low leakage current in reverse bias is desirable [46-49]. This was $>10^4$ for all temperatures measured, as shown in Figure 5.

As shown in Figure 6, at lower voltages, reverse bias leakage current is dominated by thermionic field emission (TFE) [38, 39], which is dependent on ambient temperature. However, with increasing voltage and hence electric field, the carrier tunneling and other conduction processes becomes predominant, and the leakage currents become more sensitive to temperature changes [50]. The leakage current shows a good fit to the TFE model when the reverse voltage is less than 80 V in Figure 6, and it is affected by the tunneling effect when voltage is higher than 80 V. However, the transition voltage from thermionic emission to tunneling effect did not follow the universal monotonic temperature [38,39]. The transition voltage actually decreased as the temperature increased, as illustrated in Figure 7, showing that impact ionization is not the breakdown mechanism, since that should exhibit positive temperature coefficient [46]. The variation of V_B with temperature can be represented by a relation of the form [47] :

$$V_B = V_{B0}\,[1 + \beta(T - T_0\,)]$$

where $\beta = -3.4 \pm 1.4$ V. K^{-1}. We have previously found that current increases in vertical geometry Ga_2O_3 rectifiers during electron beam induced current measurements are dominated by impact ionization of deep acceptors in the depletion region. At room temperature, mobile hole diffusion in the quasi-neutral region of Schottky diodes contributes significantly to the charge collection efficiency [48]. Electron beam induced current measurements indicated a strong amplification of photocurrent in rectifiers, attributed to the Schottky barrier lowering by holes trapped on acceptors near the surface [49].

The breakdown fields calculated from the observed breakdown voltages at different temperatures were 5.0 x10^5 V/cm at 600K, 6.3 x10^5V/cm at 500K and 9. 8x10^5 V/cm at 400K. These were obtained from the non-punch through relation E_{bd} =[$(2eN_dV_{bd})/\varepsilon]^{0.5}$ [50]. Currently, all Ga_2O_3 rectifiers show performance limited by the presence of defects and by breakdown initiated in the depletion region near the electrode corners.

When a higher reverse voltage is applied, a large number of electrons are injected into the drift region, and the current shows an $I \propto V^n$ relationship with the voltage, indicating a trap-assisted space-charge-limited conduction (SCLC) mechanism [51, 52]. Under this mechanism, a current hump should be observed before the trap-filled limited voltage, and with electrons continue to be injected into the drift region, it will lead to a breakdown. This is commonly reported in GaN, ie. the logarithmic I-V curve shows that the current I is proportional to V^n until a hump (sharp transition in I-V curve) at some threshold voltage. Such behavior can be modeled by a space-charge-limited current (SCLC) conduction mechanism with traps [53,54]. Under reverse bias and below this threshold, electrons injected into the drift layer partly contribute to conduction current and are partly captured by acceptor traps known to be present. The hump threshold voltage represents the trap-filled-limited voltage of the acceptor traps, suggesting the applied voltage overcomes the negative potential formed by the un-neutralized electrons in traps and the ionized donors in the n-Ga_2O_3. [53,54]. This shows an SCLC relation when the reverse voltage is larger than 400 V for 500 K and 600 K in Figure 7.

The reverse current characteristics at different temperatures are shown in more detail in Figure 8 (top), with all showing $I \propto V^n$ relationship. A fit to the data for the 600K reverse current characteristic is shown at the bottom of Figure 8. The data fits well to a relationship $I \propto V^n$, where n is 5.2 and the constant of proportionality is 7.6 x10^{-23}. The associated trap energies for these two regions were extracted as 0.2 and 0.4 eV from an Arrhenius plot, as shown in Figure 9. Levels with these activation energies have been reported previously in epitaxial Ga_2O_3, but were ascribed to unknown impurities and native point defects, respectively, with no specific information on their microstructure [55].

The record high reverse breakdown at high temperature in this work is a significant advance for high temperature switching applications for β-Ga_2O_3, as shown in the reverse breakdown performance when compared with previous reported works at elevated temperature in Figure 10.

Summary and Conclusions

Ultrawide bandgap semiconductors offer higher switching frequencies, higher operating temperatures and lower losses that improve power conversion efficiency. The remaining challenges and new opportunities for Ga_2O_3 in high power applications ranging from electric vehicles, medium voltage motor drives, renewable energy interfaces, microgrids, to emerging applications such as electric propulsion for aircraft include more thermally stable contacts, development of stable MOS gates, optimized edge termination and continued improvements in epi and bulk growth. For EV motor drives, the improved efficiency of ultra wide bandgap semiconductor devices would enable either extended range for the vehicle for a given battery charge, or a reduction in the battery pack required to go a certain distance. The required power modules would need large area MOSFETs delivering current in the range of 80-120 Amps per chip at 650 V to 1200 V. The promising results from vertical Ga_2O_3 rectifiers reported previously in terms of breakdown voltages and now high temperature operation suggest that thermal management issues become more important to address.

Data Availability Statement

All data that support the findings of this study are included within the article (and any supplementary files)

Acknowledgments

The work at UF was performed as part of Interaction of Ionizing Radiation with Matter University Research Alliance (IIRM-URA*)*, sponsored by the Department of the Defense, Defense Threat Reduction Agency under award HDTRA1-20-2-0002. The content of the information does not necessarily reflect the position or the policy of the federal government, and no official endorsement should be inferred. The work at UF was also supported by NSF DMR 1856662 (James Edgar). The work at NRL was supported by the Office of Naval Research.

References

1. J. Millán, P. Godignon, X. Perpiñà, A. P. Tomás, and J. Rebollo, A survey of wide bandgap power semiconductor devices, IEEE Trans. Power Electron., 29, 2155 (2014).

2. Y. Zhao and T. Palacios, Ultra Wide Bandgap Vertical Power FinFETs, IEEE Trans. Electron Dev.67, 3960 (2021).

3. A.Q. Huang, Power semiconductor devices for smart grid and renewable energy systems, Proc IEEE, 105, 2019 (2017).

4. M. Higashiwaki, Kohei Sasaki, Hisashi Murakami, Yoshinao Kumagai, Akinori Koukitu, Akito Kuramata, Takekazu Masui and Shigenobu Yamakoshi, Recent progress in Ga_2O_3 power devices, Semicond. Sci. Technol., 31, 034001 (2016).

5. S. Fujita, Wide-bandgap semiconductor materials: For their full bloom,Japan. J. Appl. Phys., 54. 030101 (2015).

6. S. J. Pearton, J. Yang, P. H. Cary, F. Ren, J. Kim, M. J. Tadjer, and M.A. Mastro, A review of Ga_2O_3 materials, processing, and devices, Appl. Phys. Rev., 5, 011301 (2018).

7. N. Allen, Ming Xiao, Xiaodong Yan, Kohei Sasaki, Marko J. Tadjer, Jiahui Ma, Ruizhe Zhang, Han Wang and Yuhao Zhang, Vertical Ga_2O_3 Schottky Barrier Diodes with Small-Angle Beveled Field Plates: A Baliga's Figure-of-Merit of 0.6 GW/cm^2,"IEEE Electron Dev. Lett., 40, 1399 (2019).

8. K. Konishi, K. Goto, H. Murakami, Y. Kumagai, A. Kuramata, S. Yamakoshi, and M. Higashiwaki, 1-kV vertical Ga_2O_3 field-plated Schottky barrier diodes, Appl. Phys. Lett. 110, 103506 (2017).

9. S. J. Pearton, F. Ren, M. Tadjer, and J. Kim, Perspective: Ga_2O_3 for ultra-high power rectifiers and MOSFETS, J. Appl. Phys. 124, 220901 (2018).

10. Samuel James Bader, Hyunjea Lee, Reet Chaudhuri, Shimin Huang, Austin Hickman, Alyosha Molnar, Huili Grace Xing, Debdeep Jena, Han Wui Then, Nadim Chowdhury, Tomás Palacios, Prospects for Wide Bandgap and Ultrawide Bandgap CMOS Devices, IEEE Trans. Electron Dev. 67, 4010 (2020).

11. Z. Hu, Hong Zhou, Qian Feng, Jincheng Zhang, Chunfu Zhang, Kui Dang, Yuncong Cai, Zhaoqing Feng, Yangyang Gao, Xuanwu Kang, Yue Hao, Field-plated lateral β-Ga_2O_3 Schottky barrier diode with high reverse blocking voltage of more than 3 kV and high DC power figure-of-merit of 500 MW/cm^2, IEEE Electron Dev. Lett., 39, 1564 (2018).

12. W. Li, K. Nomoto, Z. Hu, D. Jena, and H. G. Xing, Field-Plated Ga_2O_3 Trench Schottky Barrier Diodes with a BV^2/ Ron of up to 0.95 GW/cm^2,IEEE Electron Dev. Lett., 41, 107 (2020).

13. W. Li, K. Nomoto, Z. Hu, T. Nakamura, D. Jena, and H. G. Xing, Single and multi-fin normally-off Ga_2O_3 vertical transistors with a breakdown voltage over 2.6 kV, in 2019 IEEE International Electron Devices Meeting (IEDM), Dec. 2019, p. 12.4.1-12.4.4.

14. M. Ji, Neil R. Taylor, Ivan Kravchenko, Pooran Joshi, Tolga Aytug, Lei R. Cao, M. Parans Paranthaman, Demonstration of Large-Size Vertical Ga_2O_3 Schottky Barrier Diodes, IEEE Trans. Power Electron., 36, 41 (2021).

15. J.C. Yang, F. Ren, M.J. Tadjer, S.J. Pearton and A. Kuramata, 2300V reverse breakdown voltage Ga_2O_3 Schottky rectifiers, ECS J. Solid State Sci. Technol., 7, Q92 (2018).

16. Jiancheng Yang, Fan Ren, YenTing Chen, Yu Te Liao, Chin Wei Chang, Jenshan Lin, Marko J. Tadjer, S. J. Pearton and Akito Kuramata, Dynamic Switching Characteristics of 1 A Forward Current Ga_2O_3 Rectifiers, J. Electron. Dev. Soc. 7, 57 (2019).

17. Yangyang Gao, Ang Li, Qian Feng, Zhuangzhuang Hu, Zhaoqing Feng, Ke Zhang, Xiaoli Lu, High-Voltage β-Ga_2O_3 Schottky Diode with Argon-Implanted Edge Termination, Nanoscale Res. Lett.14, 8 (2019).

18. Z. Hu, Yuanjie Lv, Chunyong Zhao, Qian Feng Zhaoqing Feng, Kui Dang, Xusheng Tian, Yachao Zhang, Jing Ning, Hong Zhou, Xuanwu Kang, Jincheng Zhang and Yue Hao, Beveled fluoride plasma treatment for vertical -Ga_2O_3 Schottky barrier diode with high reverse blocking voltage and low turn on voltage, IEEE Electron Dev. Lett., 4 441 (2020).

19. J. Yang, Minghan Xian, Patrick Carey, Chaker Fares, Jessica Partain, Fan Ren, Marko Tadjer, Elaf Anber, Dan Foley, Andrew Lang, James Hart, James Nathaniel, Mitra L Taheri, SJ Pearton, Akito Kuramata, Vertical geometry 33.2 A, 4.8 MW cm^2 Ga_2O_3 field-plated Schottky rectifier arrays, Appl. Phys. Lett., 114, 232106 (2019).

20. C. Buttay, H.-Y. Wong, B. Wang, M. Xiao, C. DiMarino, and Y. Zhang, Surge Current Capability of Ultra-Wide-Bandgap Ga_2O_3 Schottky Diodes, Microelectron. Reliab., 114, 113743 (2020).

21. Hongpeng Zhang, Lei Yuan , Xiaoyan Tang, Jichao Hu, Jianwu Sun, Yimen Zhang, Yuming Zhang and Renxu Jia, Progress of ultra-wide bandgap Ga_2O_3 semiconductor materials in power MOSFETs, IEEE Trans Power Electronics 35, 5157 (2020).

22. Ming Xiao, Boyan Wang, Jingcun Liu, Ruizhe Zhang, Student Zichen Zhang, Chao Ding, Shengchang Lu, Kohei Sasaki, Guo-Quan Lu, Cyril Buttay, and Yuhao Zhang, Packaged Ga_2O_3 Schottky Rectifiers with Over 60 A Surge Current Capability, IEEE Power Electron. Lett (2021). doi: 10.1109/TPEL.2021.3049966.

23. K. Sasaki, Daiki Wakimoto, Quang Tu Thieu, Yuki Koishikawa, Akito Kuramata, Masataka Higashiwaki and Shigenobu Yamakoshi., First demonstration of Ga_2O_3 trench MOS-type Schottky barrier diodes, IEEE Electron Dev. Lett., 38, 783 (2017).

24. Q. He, Wenxiang Mu, Bo Fu, Zhitai Jia, Shibing Long, Member, IEEE, Zhaoan Yu, Zhihong Yao, Wei Wang, Hang Dong, Yuan Qin, Guangzhong Jian, Ying Zhang, Huiwen Xue, Hangbing Lv, Qi Liu, Minghua Tang, Xutang Tao and Ming Liu, Schottky barrier rectifier based on (100) β-Ga_2O_3 and its DC and AC characteristics, IEEE Electron Dev. Lett., 39, 556 (2018).

25. Z. Hu, Hong Zhou, Qian Feng, Jincheng Zhang, Chunfu Zhang, Kui Dang, Yuncong Cai, Zhaoqing Feng, Yangyang Gao, Xuanwu Kang , and Yue Hao, Field-plated lateral β-Ga_2O_3 Schottky barrier diode with high reverse blocking voltage of more than 3 kV and high DC power figure-of-merit of 500 MW/cm^2, IEEE Electron Dev. Lett., 39, 1567 (2018)

26. H. Zhou, M. Si, S. Alghamdi, G. Qiu, L. Yang, and P. D. Ye, High- performance depletion/enhancement-ode β-Ga_2O_3 on insulator (GOOI) field-effect transistors with record drain currents of 600/450 mA/mm, IEEE Electron Dev. Lett., 38, 103 (2017)

27. Tatsuro Watahiki, Yohei Yuda, Akihiko Furukawa, Mikio Yamamuka, Yuki Takiguchi, and Shinsuke Miyajima, Heterojunction p-Cu_2O/n-Ga_2O_3 diode with high breakdown voltage Appl. Phys. Lett. 111, 222104 (2017).

28. Weibing Hao, Qiming He, Kai Zhou, Guangwei Xu, Wenhao Xiong, Xuanze Zhou, Guangzhong Jian, Chen Chen, Xiaolong Zhao, and Shibing Long, Low defect density and small curve hysteresis in NiO/β-Ga_2O_3 pn diode with a high PFOM of 0.65 GW/cm^2, Appl. Phys. Lett. 118, 043501 (2021).

29. Y. Kokubun, S. Kubo, and S. Nakagomi, All-oxide p–n heterojunction diodes comprising p-type NiO and n-type β-Ga_2O_3, Appl. Phys. Express. 9, 091101 (2016).

30. T. Watahiki, Y. Yuda, A. Furukawa, M. Yamamuka, Y. Takiguchi, and S.Miyajima, Heterojunction p-Cu_2O/n-Ga_2O_3 diode with high breakdown voltage, Appl. Phys. Lett. 111, 222104 (2017).

31. S-i Kan, S. Takemoto, K. Kaneko, I. Takahashi, M. Sugimoto, T. Shinohe, and S. Fujita, Electrical properties of α-Ir_2O_3/α-Ga_2O_3 pn heterojunction diode and band alignment of the heterostructure, Appl. Phys. Lett. 113, 212104 (2018).

32. J. C. Gallagher, A. D. Koehler, M. J. Tadjer, N. A. Mahadik, T. J. Anderson, S. Budhathoki, K.-M. Law, A. J. Hauser, K. D. Hobart, and F. J. Kub, Demonstration of CuI as a P–N heterojunction to *β*-Ga_2O_3, Appl. Phys. Express. 12, 104005 (2019).

33. S. Ghosh, M. Baral, R. Kamparath, R. J. Choudhary, D. M. Phase, S. D. Singh and T. Ganguli, Epitaxial growth and interface band alignment studies of all oxide α-Cr_2O_3/β-Ga_2O_3 p-n heterojunction, Appl. Phys. Lett. 115, 061602 (2019).

34. X. Lu, X. Zhou, H. Jiang, K. W. Ng, Z. Chen, Y. Pei, K. M. Lau, and G. Wang, 1-kV Sputtered p-NiO/n-Ga_2O_3 Heterojunction Diodes With an Ultra-Low Leakage Current Below 1 μ A/cm^2, IEEE Electron Dev. Lett. 41, 449 (2020).

35. Yuanjie Lv, Yuangang Wang, Xingchang Fu, Shaobo Dun, Zhaofeng Sun, Hongyu Liu, Xingye Zhou, Xubo Song, Kui Dang, Shixiong Liang, Jincheng Zhang, Hong Zhou, Zhihong Feng, Shujun Cai, and Yue Hao, Demonstration of β-Ga_2O_3 Junction Barrier Schottky Diodes with a Baliga's Figure of Merit of 0.85 GW/cm^2 or a 5A/700 V Handling Capabilities, IEEE Trans. Power Electron. (2020).

36. H.H. Gong, X. H. Chen, Y. Xu, F.-F. Ren, S. L. Gu, and J. D. Ye, A 1.86-kV double-layered NiO/*β*-Ga_2O_3 vertical p–n heterojunction diode, Appl. Phys. Lett. 117, 022104 (2020).

37. Ribhu Sharma, Minghan Xian, Chaker Fares, Mark E. Law, Marko Tadjer, Karl D. Hobart, Fan Ren and S. J. Pearton, Effect of probe geometry during measurement of >100 A Ga_2O_3 vertical rectifiers, J. Vac. Sci. Technol. A 39, 013406 (2021).

38. Boyan Wang, Ming Xiao, Xiaodong Yan, Hiu Yung Wong, Jiahui Ma, Kohei Sasaki, Han Wang and Yuhao Zhang, High-voltage vertical Ga_2O_3 power rectifiers operational at high temperatures up to 600 K, Appl. Phys. Lett., 115, 263503 (2019).

39. Wenshen Li, Kazuki Nomoto, Debdeep Jena and Huili Grace Xing, Thermionic emission or tunneling? The universal transition electric field for ideal Schottky reverse leakage current: A case study in β-Ga_2O_3, Appl. Phys. Lett. 117, 222104 (2020).

40. S. Rafique, L. Han, S. Mou and H. Zhao, Temperature and doping concentration dependence of the energy band gap in β-Ga_2O_3 thin films grown on sapphire, Optical Mater Express 7, 3561 (2017).

41. Jürgen H. Werner and Herbert H. Güttler, Temperature dependence of Schottky barrier heights on silicon, J Appl. Phys. 73, 1315 (1993).

42. Luke A. M. Lyle, Kunyao Jiang, Elizabeth V. Favela, Kalyan Das, Andreas Popp and Zbigniew Galazka, Guenter Wagner, and Lisa M. Porter, Effect of metal contacts on (100) β-Ga_2O_3 Schottky, J. Vac. Sci. Technol. A 39, 033202 (2021).

43. Tsung-Han Yang, Houqiang Fu, Hong Chen, Xuanqi Huang, Jossue Montes, Izak Baranowski, Kai Fu and Yuji Zhao, Temperature-dependent electrical properties of β-Ga_2O_3 Schottky barrier diodes on highly doped single-crystal substrates. J. Semicond. 40, 012801 (2019).

44. S. K. Cheung and N. W. Cheung, Appl. Phys. Lett. 49, 85 (1986).

45. Manoj K Yadav, Arnab Mondal, Satinder K. Sharma and Ankush Baga, Substrate orientation dependent current transport mechanisms in β-Ga_2O_3/Si based Schottky barrier diodes, J. Vac. Sci. Technol. A 39, 033203 (2021).

46. Lina Cao, Jingshan Wang, Galen Harden, Hansheng Ye, Roy Stillwell, Anthony J. Hoffman, and Patrick Fay, Experimental characterization of impact ionization coefficients for electrons and holes in GaN grown on bulk GaN substrates, Applied Physics Lett. 112, 262103 (2018).

47. C. Kizilyalli, A. P. Edwards, O. Aktas, T. Prunty, and D. Bour, Vertical Power p-n Diodes Based on Bulk GaN, IEEE Trans. Electron Devices 62, 414 (2015).

48. E.B. Yakimov, A.Y. Polyakov, N. B. Smirnov, I.V. Shchemerov, P.S. Vergeles, E.E. Yakimov, A.V. Chernykh, Minghan Xian, F. Ren and S.J. Pearton, Role of Hole Trapping by Deep Acceptors in Electron Beam Induced Current Measurements in β-Ga_2O_3 Vertical Rectifiers, J. Phys. D. 53, 495108 (2020).

49. E.B Yakimov, A.Y Polyakov, I.V Shchemerov, N.B Smirnov, A.A Vasilev, P.S Vergeles, E.E Yakimov, A.V Chernykh, A.S Shikoh, F Ren, S.J. Pearton, Photosensitivity of Ga_2O_3 Schottky diodes: Effects of deep acceptor traps present before and after neutron irradiation, APL Mater. 8, 111105 (2020).

50. Robert Kaplar, Oleksiy Slobodyan, Jack Flicker, Jeramy Dickerson, Trevor Smith1, Andrew Binder and Mark Hollis, Analysis of the Dependence of Critical Electric Field on Semiconductor Bandgap, presented at 236TH ECS Meeting, Atlanta, GA, October 13-17, 2019

51. Rahul Radhakrishnan, Tony Witt, and Richard Woodin, Temperature Dependence Design of Silicon Carbide Schottky Diodes, in 2nd IEEE Workshop Wide Bandgap Power Devices Appl. WiPDA 2014 (IEEE, 2014), pp. 151–154.

52. M. Xiao, Tomás Palacios and Yuhao Zhang, Leakage and breakdown mechanisms of GaN vertical power FinFETs, Appl. Phys. Lett. 114, 163503 (2019).

53. C. Zhou, Q. Jiang, S. Huang, and K. J. Chen, Vertical Leakage/Breakdown Mechanisms in AlGaN/GaN on Si Devices, IEEE Electron Device Lett., 33, 1132 (2012).

54. Y. Yoshizumi, S. Hashimoto, T. Tanabe, and M. Kiyama, High breakdown-voltage pn-junction diodes on GaN substrates, J. Cryst. Growth, 298, pp. 875 (2007).

55. Zhengpeng Wang, Xuanhu Chen, Fang-Fang Ren, Shulin Gu and Jiandong Ye, Deep-level defects in gallium oxide, J. Phys. D: Appl. Phys. 54, 043002 (2021).

56. C. Hou, K. R. York, R. A. Makin S. M. Durbin, R. M. Gazoni, R. J. Reeves and M. W. Allen, High temperature (500 °C) operating limits of oxidized platinum group metal (PtO_x, IrO_x, PdO_x, RuO_x) Schottky contacts on β-Ga_2O_3, Appl .Phys. Lett. 117, 203502 (2020).

57. S. Ahn, F. Ren, L. Yuan, S. J. Pearton, and A. Kuramata, Temperature-dependent characteristics of Ni/Au and Pt/Au Schottky diodes on β-Ga_2O_3, ECS J. Solid State Sci. Technology 6, P68 (2017).

58. M. Higashiwaki, Keita Konishi, Kohei Sasaki, Ken Goto, Kazushiro Nomura, Quang Tu Thieu, Rie Togashi, Temperature-dependent capacitance-voltage and current-voltage characteristics of Pt/Ga_2O_3 (001) Schottky barrier diodes fabricated on n-Ga_2O_3 drift layers grown by halide vapor phase epitaxy, Appl. Phys. Lett. 108, 133503 (2016).

Figure Captions

Figure 1. Nomarski microscope images of the HVPE layers before (top, left and right) and after subsequent polishing to planarize the surface (bottom, left and right).

Figure 2. Schematic of vertical rectifier structure (top) and photograph of fabricated β-Ga_2O_3 Schottky diode array with 40µm×40µm squares (bottom).

Figure 3. Forward I-V characteristic for rectifiers as a function of temperature.

Figure 4. Schottky barrier height and ideality factor retrieved from diode forward I-V as a function of temperature.

Figure 5. On/off ratio when switching from 2 V forward bias to the reverse biases shown on the x-axes at various temperatures.

Figure 6. Reverse current density of the vertical β-Ga_2O_3 Schottky diode at various temperatures fitted to the TFE model for reverse biases of 5-100 V.

Figure 7. Reverse I-V-T characteristics at 400-600 K for rectifiers at various temperatures.

Figure 8. Experimental data for reverse current characteristics at 400-600K and fit to an $I \propto V^n$ relationship (top) and more detailed view of 600K reverse current characteristic and fit to an $I \propto V^n$ relationship with n=5.2 (bottom).

Figure 9. Arrhenius plot ΔI/ΔV versus 1/T. The *I-V* slope of the voltages ranges from 200-400 V, and ranges over 400 V for rectifiers measured as a function of temperature.

Figure 10. Comparison of operation temperature versus maximum reverse bias for reported vertical Ga_2O_3 rectifiers. Previous data comes from Virginia Tech [38], University of Canterbury [56], University of Florida [57] and NIICT [58].

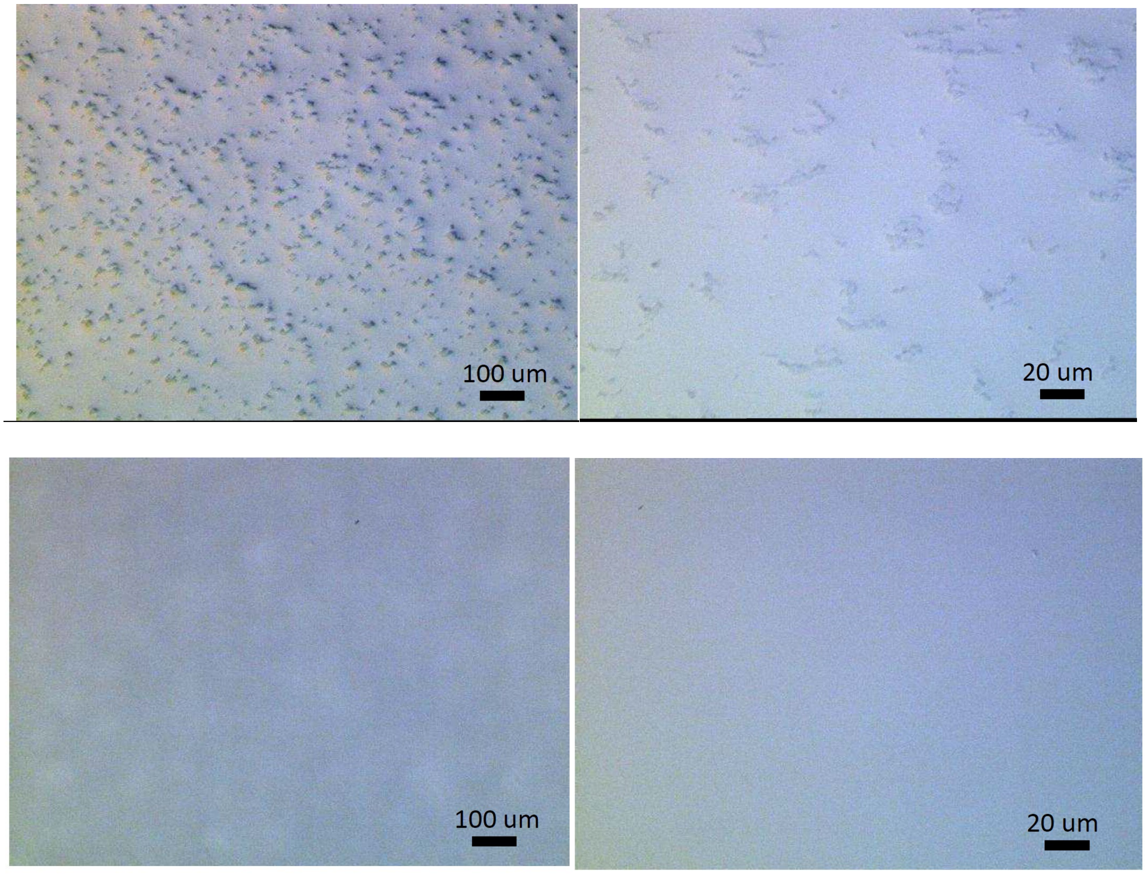
100 um
20 um
100 um
20 um

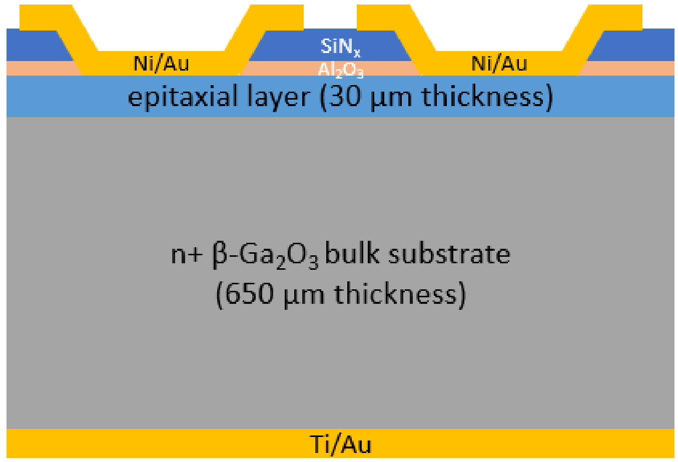
SiN$_x$
Ni/Au
Al_2O_3
Ni/Au
epitaxial layer (30 μm thickness)
n+ β-Ga_2O_3 bulk substrate
(650 μm thickness)
Ti/Au

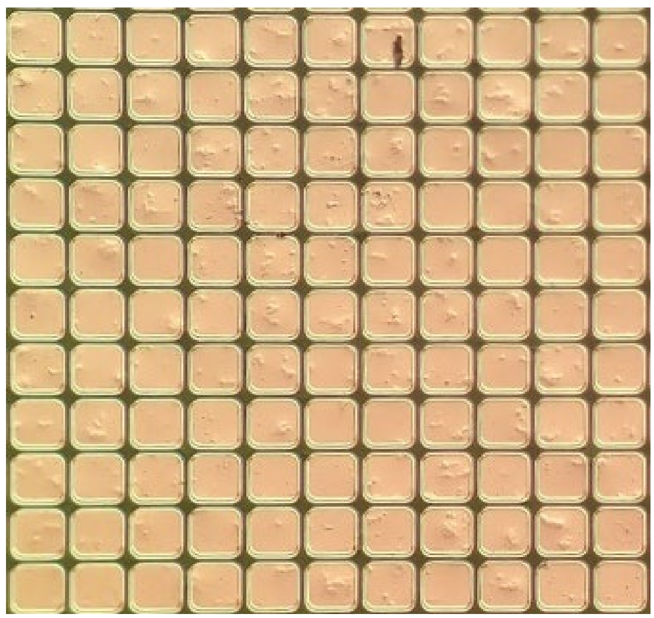

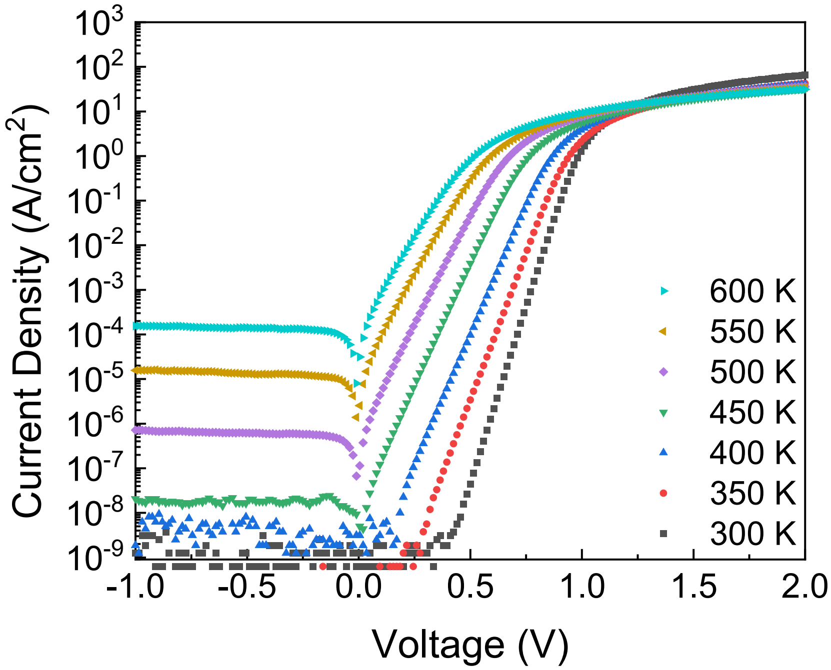
Current Density (A/cm²)
10³
10²
10¹
10⁰
10⁻¹
10⁻²
10⁻³
10⁻⁴
10⁻⁵
10⁻⁶
10⁻⁷
10⁻⁸
10⁻⁹
-1.0
-0.5
0.0
0.5
1.0
1.5
2.0
Voltage (V)
600 K
550 K
500 K
450 K
400 K
350 K
300 K

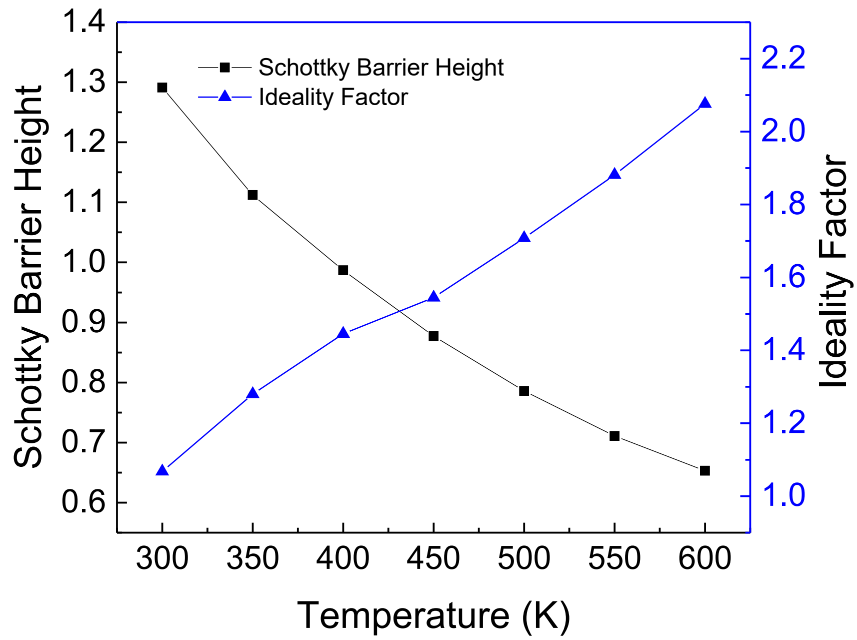
Schottky Barrier Height
Ideality Factor
1.4
1.3
1.2
1.1
1.0
0.9
0.8
0.7
0.6
2.2
2.0
1.8
1.6
1.4
1.2
1.0
300
350
400
450
500
550
600
Temperature (K)
Schottky Barrier Height
Ideality Factor

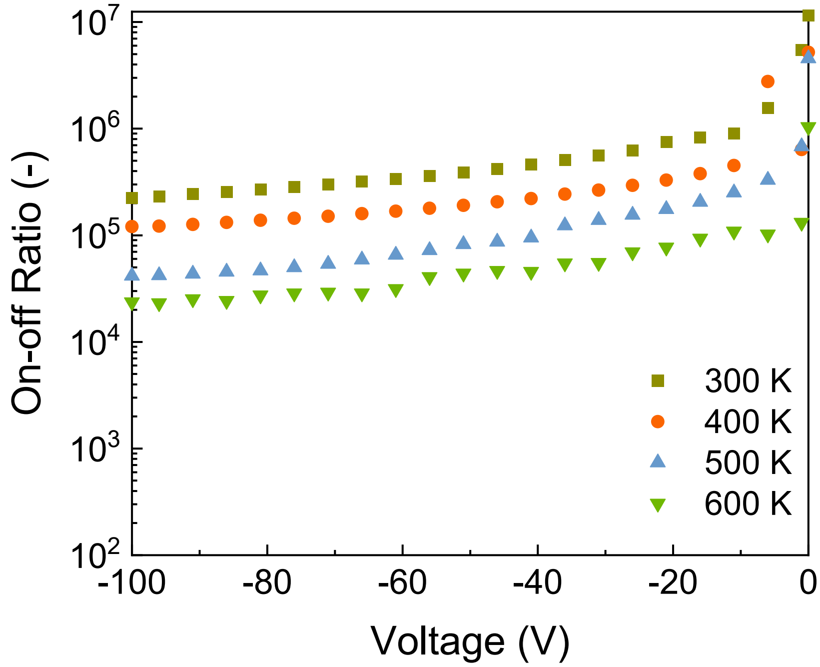

On-off Ratio (-)
10^7
10^6
10^5
10^4
10^3
10^2
-100
-80
-60
-40
-20
0
Voltage (V)
300 K
400 K
500 K
600 K

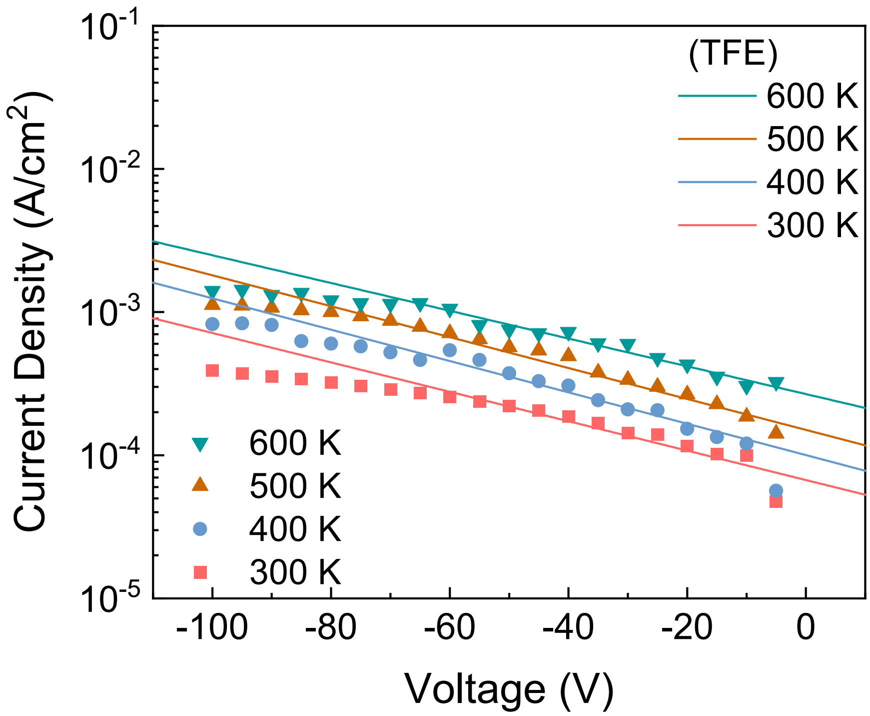
(TFE)
600 K
500 K
400 K
300 K
600 K
500 K
400 K
300 K
Current Density (A/cm^2)
10^{-1}
10^{-2}
10^{-3}
10^{-4}
10^{-5}
-100
-80
-60
-40
-20
0
Voltage (V)

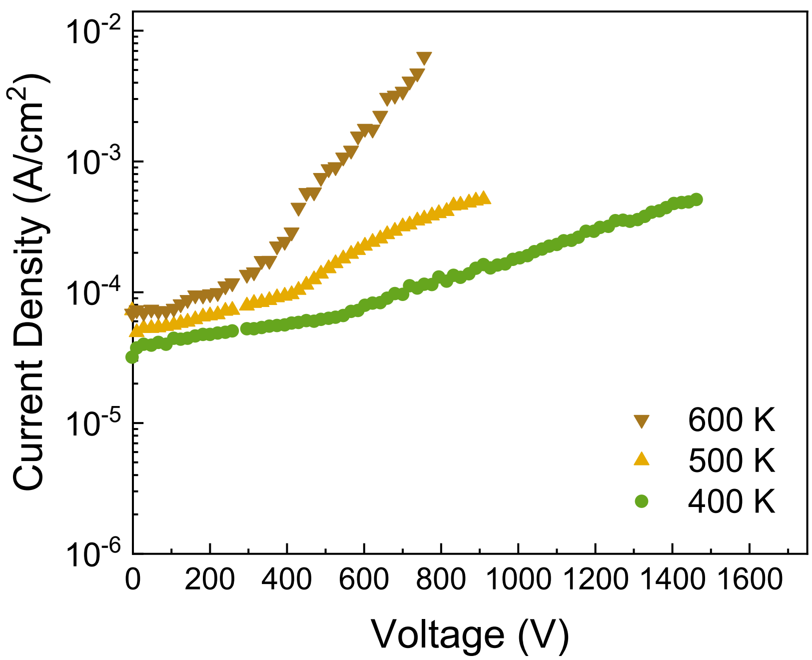

Current Density (A/cm2)
10-2
10-3
10-4
10-5
10-6
0
200
400
600
800
1000
1200
1400
1600
Voltage (V)
600 K
500 K
400 K

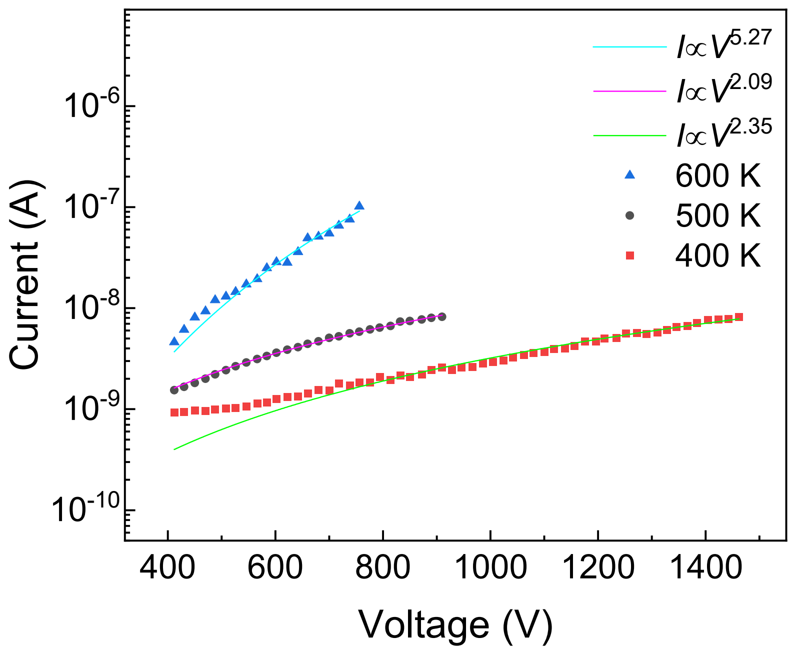

I∝V^5.27
I∝V^2.09
I∝V^2.35
600 K
500 K
400 K
Current (A)
10^-6
10^-7
10^-8
10^-9
10^-10
400
600
800
1000
1200
1400
Voltage (V)

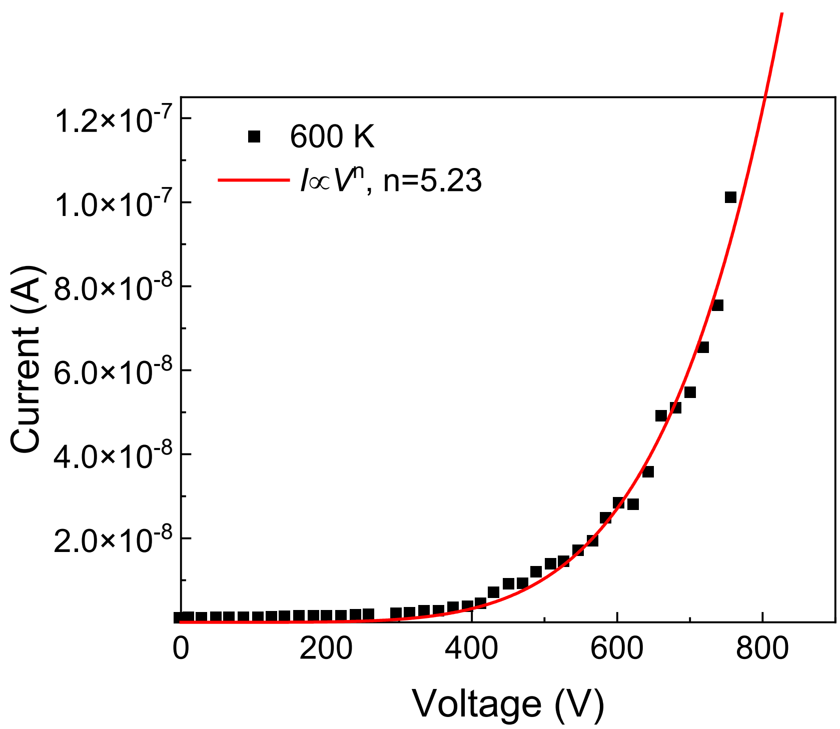

600 K
I∝V^n, n=5.23
Current (A)
1.2×10^-7
1.0×10^-7
8.0×10^-8
6.0×10^-8
4.0×10^-8
2.0×10^-8
0
200
400
600
800
Voltage (V)

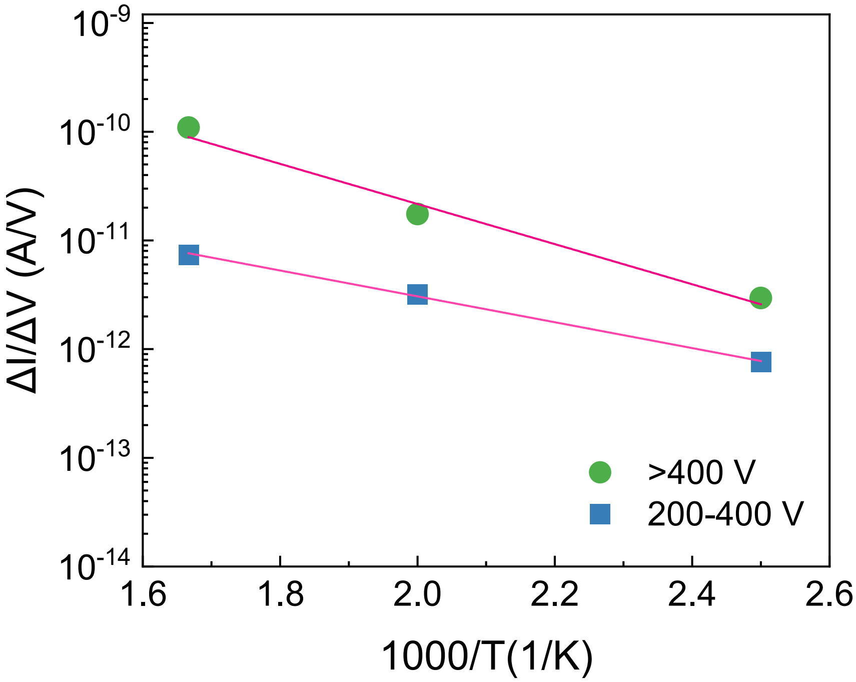
10^-9
10^-10
10^-11
10^-12
10^-13
10^-14
ΔI/ΔV (A/V)
1.6
1.8
2.0
2.2
2.4
2.6
1000/T(1/K)
>400 V
200-400 V

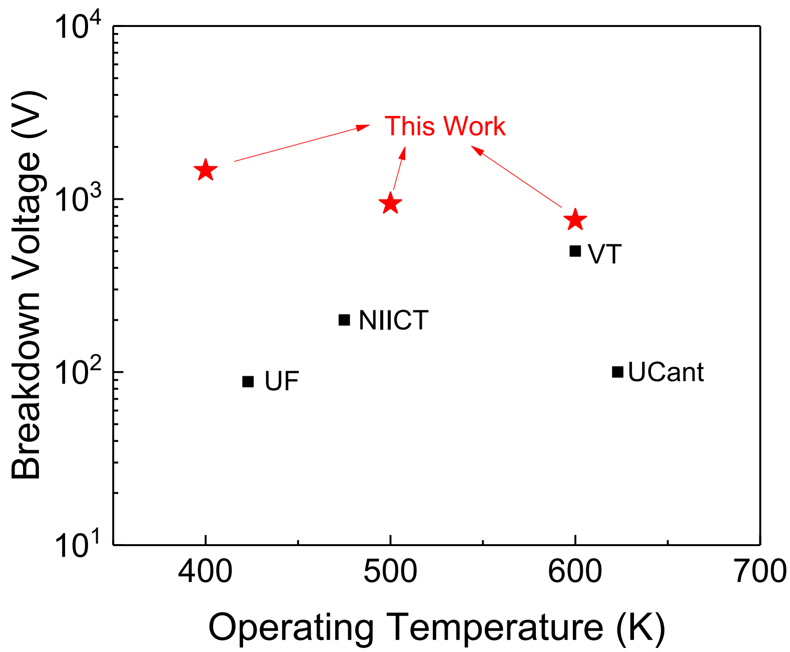
This Work
VT
NIICT
UF
UCant
10^4
10^3
10^2
10^1
400
500
600
700
Breakdown Voltage (V)
Operating Temperature (K)